JOURNAL OF COMPUTATIONAL PHYSICS 73, 85–106 (1987)

Integrated Analysis of Data from JET

J. P. CHRISTIANSEN

Theory Division, JET Joint Undertaking, Abingdon, Oxfordshire OX14 3EA, England

Received March 14, 1986; revised September 29, 1986

A series of computational techniques are applied to interpret diagnostic data from JET (the joint European torus). Some of these techniques are applied in parallel by packages which produce results that can be integrated by other packages. The associated data flow starts from raw measurements stored in JPFs (JET pulse files) and runs through a hierarchy of PPFs (processed pulse files) containing calculated results. A small subset of these are extracted into a data bank and employed for statistical studies such as scaling laws. Examples of computational techniques and calculated results are given together with an overview of the organisation of data flow and code structures. © 1987 Academic Press, Inc.

INTRODUCTION

Large tokamaks such as JET, TFTR, and JT60 collect substantial amounts of data during a single plasma pulse; in the case of JET presently 7 Mbytes of data are produced per pulse and the amount will be increased to 10 Mbytes. In other areas of physics large amounts of data are collected per observation or per experiment; for example, in the case of a seismic investigation up to 100 Gbytes may be produced. In plasma physics eperiments the data from a plasma pulse represents a diversity of physics measurements. On JET the 7 Mbytes are divided into 2 Mbytes of "machine parameters" and 5 Mbytes of data from a wide range of diagnostic measurements. Approximately 1 Mbyte of the JET data (mainly diagnostic data) is used for regular analysis after each pulse. In this paper we describe some aspects of the data analysis methods and the associated organization of data flow based on the articles in Ref. [1, 2].

At most of the fusion laboratories in Europe and the United States data analysis, data storage, and data management on present fusion experiments are based on the experience from previous experiments. For some diagnostic methods this experience dates back more than one decade. Sometimes data from two separate diagnostics are not available on a single computer and to integrate the data analysis from the two diagnostics may become a time consuming exercise. All the data from a single pulse on JET are assembled into a single pulse file, the *JET pulse file* or JPF. All JPFs are stored on a mass store at the AERE Harwell computer centre. Section 1 of this paper will describe the flow of data from these JPFs through analysis programs

0021-9991/87 $3.00

and into other disc files and data banks. The data flow on JET for a given pulse may terminate at one of four levels of analysis depending on the type of pulse and on the availability of diagnostic data. The remaining sections of this paper will follow the analysis methods to the final level at which the overall performance of JET is assessed. This assessment involves mainly the dependence of confinement properties on plasma physics parameters such as field, current, plasma density, plasma geometry, auxiliary heating.

Additional topics, such as impurity studies, effects of sawteeth, plasma fuelling, MHD instabilities, disruptions, are pursued using mainly the results from the intermediate analysis levels.

The organisation of the data flow is based on a file storage system, the PPF (*p*rocessed *p*ulse *f*ile) system developed at JET by R. T. Ross; the details of this system and further details of the analysis described in this paper can be found in the JET reports of Ref. [2]. Each of the computer programs which regularly analyse JET data can access not only the raw data in the JPFs, but through a standard subroutine interface they access results stored in the PPFs. Many other computational facilities in use within JET, e.g., graphical display of data and results, make use of the PPF standard interface. Thus the problems associated with interfacing different types of computer programs are overcome by the adoption of single standard file storage system. The integrated analysis of JET data from a single pulse is carried out by a computer program which accesses the JPF and all the PPFs produced for that pulse; the results are themselves stored in a PPF. To integrate the analysis for many JET pulses (1000 or more) the PPFs are accessed in groups of 10 or 20 and the results carefully checked by a physicist before data extraction to a data base takes place.

The data flow on JET is explained in Section 1 and shown graphically in Fig. 1; it starts from a simple magnetic analysis which is outlined briefly in Section 2; this simple analysis is carried out for all plasma pulses. Section 3 describes the methods for identifying the plasma position and shape; plasma boundary identification is done for pulses with a plasma current above 1 MA by a code called FAST. Section 4 deals with some computational techniques applied to the data from a variety of JET diagnostics and it is explained how the global confinement analysis is carried out by a code called INDIANA. Representative results from the analysis are given in Section 5. In Section 6 some features of the 2 main analysis codes FAST (*f*ast *a*nalysis with *s*imple *t*opology) and INDIANA (*in*tegrated *d*ata *i*nterpretation *ana*lysis) are described. Both these codes are based on an extension of the OLYMPUS system [1] originally developed by Keith Roberts and the author. Indeed, many techniques used in the integrated data analysis on JET owe much to the influence from Keith Roberts with whom the author worked for 15 years.

1. The JET Data Flow

Figure 1 presents a rough summary of the flow of JET data for a single plasma

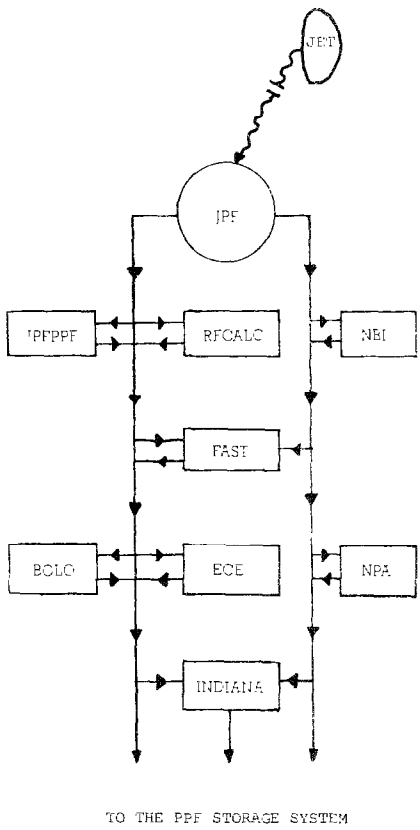

FIG. 1. Flow of JET data from the JET pulse file through interpretation codes which store their data on PPFs (Table II). The results are extracted to data banks.

pulse from the JPF through 8 interpretation codes to various PPFs. From these PPFs a small subset (<0.5%) is selected for each pulse and carefully checked before this data subset is transferred to a data bank which contains similar data subsets from many other pulses. This data bank is not shown in Fig. 1. During operation of the JET tokamak a set representative results from the analysis codes are ready from the PPFs and made available in graphical form shortly after each JET pulse; these graphs are studied and any gross errors in the data or calculations are taken into account and the appropriate action taken.

Table I lists those diagnostics whose data is regularly processed. Table II presents the type of results stored in the PPFs by each code. These results are grouped into so called DDAs (*d*iagnostic *d*ata *a*reas) each of which are referenced by a name. Most of the results, e.g., plasma current, are scalar functions of time and stored as 1-dimensional vectors. Other results, e.g., electron temperature T_e obtained from Electron cyclotron emission, are functions of both space and time; such results are stored as a stack of vectors $T_e(R_1, t)$, $T_e(R_2\ t)$, etc. In most cases a vector contains

TABLE I

JET Diagnostics Whose Data is Regularly Processed

1.	Magnetic	Poloidal B at 18 vessel locations.
		Flux function of 14 vessel locations
		Loop voltage
		Toroidal field and coil displacement
		Diamagnetic loop
		Poloidal field coil currents
2.	2-mm interferometer:	$\int n\,dl$ at one sightline
3.	ECE spatial scan:	Electron temperature profile in midplane
4.	Neutral particle analyser:	Central ion temperature
5.	Bolometer cameras:	Radiation at 40 viewing chords
6.	H_α monitors:	H_α emission of limiter and wall
7.	Visible bremsstrahlung:	Emission from one sightline
8.	Neutron emission:	Time resolved yield
9.	0.2-mm interferometer:	$\int n\,dl$ at seven sightlines

1000 values at 1000 discrete time values; the time values are not uniformly sampled since the sampling rate is increased during, say, auxiliary heating. A full analysis per pulse yields approximately 2 Mb of results stored in PPFs. Once the full analysis is complete, some 5–15 min after a plasma pulse, analysis of the next pulse can

TABLE II

Interpretation Codes Used regularly to Process Data from JET

Computer code	Results	PPF name
1. JPFPPF	Basic magnetic results	MAGN
	$\int$ n dl for 2-mm interferometer	MWI
	Thomson scattering (single point)	THOM
2. RFCALC	RF power, antennae load	ICRH
3. NBI	Power for each neutral beam	NBI8
4. FAST	Basic magnetic results	MG0
	RF resonance lines	CRH1
	Magnetic analysis	MG2, MG3
	Surface geometry	LAO
	Average density	DEN
5. ECE	T_e profile in midplane	ECM1
6. NPA	Central T_i. Fluxes of neutrals	NPA3
7. BOLO	Total radiation power	BOLO
8. INDIANA	Volume averaged T_e	EC2
	Density profile fitting	NEX
	Z_{eff}. Particle confinement	HAL
	Axial T_i from neutrons	TIN
	Resistive Z_{eff}	KIN
	Global power balance	KIN
9. IDENTB	Full MHD equilibrium	MAGI

Note. Their results are stored in PPFs (see text) with names as given in the last column.

commence according to circumstances. The control of the processing is triggered by the arrival of a JPF at the AERE Harwell IBM 3083 computer. Bottlenecks in this continuous data flow pattern arise only if either the high speed link between JET and AERE malfunctions or if there is an excessive load on the IBM 3083 computer.

When the processing has been completed for, say, 100 or 200 pulses corresponding to 1–3 weeks of operation, the non-automated part of the data flow takes place. This involves a physicist in a selection of a few (1 to 5) discrete time values from a study of the time dependent vectors. These discrete time values are typed into a file for each plasma pulse and a computer program starts reading through the PPFs, vector by vector to extract values used fo the study of a physics topic of interest.

If at a later stage it is discovered that some part of the JPF has been processed by the interpretation codes using an incorrect procedure, the relevant parts of the data processing will be repeated. Such a reprocessing sequence may arise if, for example, the calibration of a measurement has changed. The relevant interpretation code is then made to loop over the pulses concerned and new PPFs are generated; each PPF carries two identifiers: the pulse number and a sequence number. The PPF utility programs always access the requested PPF with the highest sequence number.

2. Simple Analysis of Magnetic Measurements

Figure 2 shows a cross section of the JET vacuum vessel; the locations are marked of 18 pickup coils measuring the tangential values B_j, $j=1,18$ of the poloidal field and of 14 flux loops measuring the flux ψ_j, $j=1,14$. A similar set of magnetic diagnostics can be found on other tokamaks, e.g., Doublet III and ISX. The analysis of the magnetic measurements described below and in the next section has a lot in common with those described in Ref. [3–9]. Reference [10] contains a paper by JET authors describing the initial analysis used during 1983. The magnetic data (B and ψ) as recorded in the JPF is first calibrated and then corrected for pickup of the toroidal field. The corrected data is used extensively in the analysis and stored in a PPF together with quantities defined below in Eq. (1) to (3).

From the data on B and ψ we find 4 extremum points of the plasma surface by Taylor expansion. For example, the top point of the plasma surface is evaluated from

$$Z(\text{Top}) = Z(\text{loop } 5) - (\psi_p - \psi(\text{loop } 5))(\partial\psi/\partial Z)^{-1}, \tag{1}$$

where $\partial\psi/\partial Z = \frac{1}{2} R(\text{coil } 5)\ (B(\text{coil } 5) + B(\text{coil } 6))$.

The value of flux ψ_p at the boundary is also found by Taylor expansion.

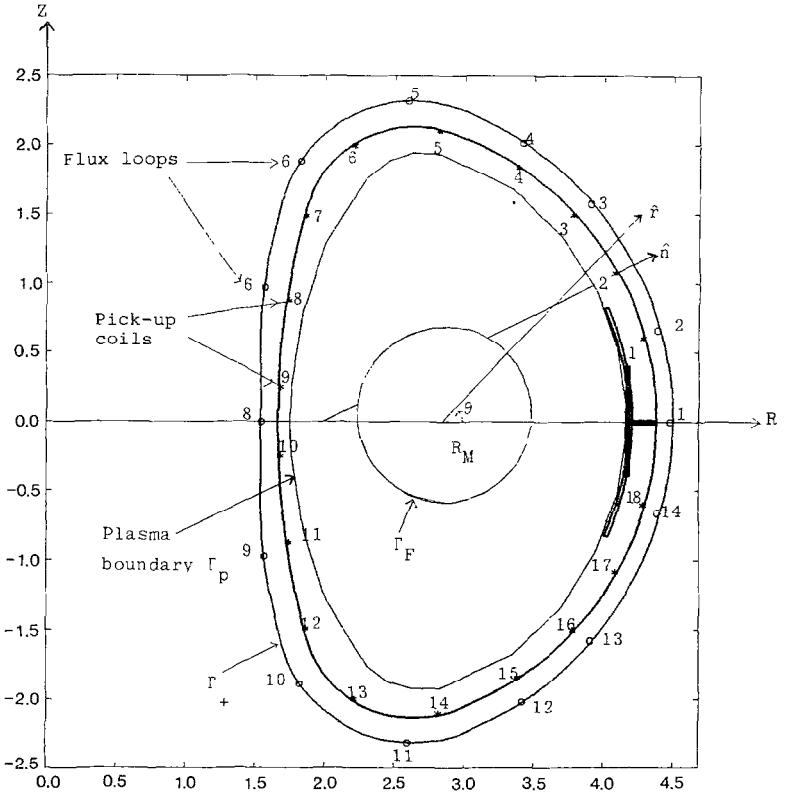

FIG. 2. JET vessel with locations of pickup coils and flux loops marked. Also shown are RF antenna and limiter. The plasma boundary Γ_p is found by a method (Section 3.2) which assumes currents to flow on surfaces Γ_F and Γ_+. The vectors n, r, and the angle θ are referred to in the text.

Integrations around the vessel are carried out following [10] and [11] to find the plasma current and 1st-order current moments

$$I=\frac{1}{\mu_0}\int B\,dl$$

$$Y_{1R}=\frac{1}{\mu_0 I}\int (R^2-R_M^2)B+2ZRB_n)\frac{1}{2}R_M\,dl \tag{2}$$

$$Y_{1Z}=\frac{1}{\mu_0 I}\int\left(ZB+R\log\frac{R_J}{R}B_n\right)dl, \qquad B_n=\frac{1}{R}\frac{\Delta\psi}{\Delta L}n.$$

The current centre (R_J, Z_J) is then (n.b. different from [11])

$$R_J=R_M\left(1+2\frac{Y_{1R}}{R_M}\right)^{1/2}, \qquad Z_J=Y_{1Z}, \tag{3}$$

where R_M is a fixed value (the torus centre). The above calculations though primitive, are useful when the method described in the next section fails to identify the plasma shape and position; this is the case in plasma breakdown studies when the current is very small.

3. Plasma Equilibrium

The calculation of an axisymmetric toroidal equilibrium from external magnetic measurements has been carried out by many authors using a variety of computation techniques. References [4–9] describe some of these and the review papers in Ref. [10] direct the reader to most of the methods in use. The method applied to JET data derives from the work of W. Feneberg, K. Lackner, and P. Martin at Garching (Section 3.1) and Ref. [12] describes in detail the computer program supplied to JET under a contract agreement. A fast method described below is used first to determine the plasma boundary. From the solution obtained several plasma parameters such as plasma β, inductance, and safety factor are found (see Section 3.2). The geometry of the plasma surface is described (Section 3.3) by the method of Lao *et al.* [13] and form the basis of the subsequent analysis methods of Section 4. Thus an approximation to the plasma equilibrium is found without solving the full Grad–Shafranov equation. The reason for this is that 1000 approximate equilibria are calculated per pulse and the computing time required for full solutions would be excessive. Comparisons between full solutions obtained by the code of Blum *et al* [10] and the approximate solutions are made regularly.

3.1. *Plasma Boundary Identification* (*W. Feneberg, K. Lackner, and P. Martin*)

The plasma boundary Γ_p is defined as that contour of constant $\psi = \psi_p$ passing through 1 of 20 "virtual limiter" points. These points are (see Fig. 2) the 18 pickup coil locations and the inner–outer vessel points at $Z = 0$. The value ψ_p is chosen as the maximum or minimum, depending on the sign of the current, from

$$\begin{aligned} \psi_p &= \mathrm{Max}(\psi_l), \qquad l = 1, 20 \ (I > 0) \\ \psi_p &= \mathrm{Min}(\psi_l), \qquad l = 1, 20 \ (I > 0). \end{aligned} \tag{4}$$

The solution $\psi(R, Z)$ is decomposed into 3 parts as

$$\psi = \psi_J + \psi_{x1} + \psi_{x2}.$$

$\psi_{x1} + \psi_{x2}$ represent the flux generated by external coils as well image currents induced by the plasma current in non-steady states. ψ_J represents the flux due to the plasma current. Inside the contour Γ_+ these functions satisfy

$$\Delta^* \psi_{x1} = 0, \qquad \Delta^* \psi_{x2} = 0, \qquad \Delta^* \psi_J = -\mu_0 R J_\phi.$$

The boundary conditions on Γ_+ are

$$\psi_{x1}(\Gamma_+) = \psi_{\text{measured}}, \qquad \psi_{x2}(\Gamma_+) + \psi_J(\Gamma_+) = 0.$$

A Greens function technique is used to determine these flux functions. The contour Γ_+ (see Fig. 2) carries a current distribution (R_+, Z_+ denote co-ordinates of Γ_+)

$$J_{x1} = \sum_0^8 I_{x1n} \cos n\theta + \sum_1^6 i_{x1n} \sin n\theta$$

with $I_{x1n} = I_{x1n}\,\delta(R - R_+, Z - Z_+)$ and $i_{x1n} = i_{x1n}\,\delta(R - R_+, Z - Z_+)$. The flux ψ_{x1} at (R, Z) due to J_x is

$$\psi_{x1}(R, Z) = \frac{\mu_0}{\pi} \int_{\Gamma_+} J_x(R_+, Z_+)\, G(R, Z, R_+, Z_+)\, dl,$$

where the Greens function is

$$G(R, Z, R_+, Z_+) = \frac{1}{R}(RR_+)^{1/2}\left(\left(1 - \frac{1}{2}k^2\right) E_1(k) - E_2(k)\right),$$

$$k^2 = \frac{4RR_+}{(R + R_+)^2 + (Z - Z_+)^2}.$$

E_1 and E_2 are the elliptic integrals of the first and second kind. The flux ψ_J at (R, Z) due to J_ϕ is

$$\psi_J(R, Z) = \frac{\mu_0}{\pi} \int_{\Gamma_F} J_\phi(R_F, Z_F)\, G(R, Z, R_F, Z_F)\, dl.$$

ψ_{x1} is found from the boundary condition

$$\psi_{x1}(R_L, Z_L) = \psi(R_L, Z_L), \qquad L = 1, 14 \text{ (flux loop location)},$$

which determines the current amplitudes I_{x1n} and i_{x1n}.

The boundary condition $\psi_J(R_L, Z_L) + \psi_{x2}(R_L, Z_L) = 0$ yields

$$\psi_{x2}(R_L, Z_L) = -\frac{\mu_0}{\pi} \int_{\Gamma_+} J_{x2}(R_+, R_+)\, G(R, Z, R_+, Z_+)\, dl.$$

The coefficients I_{x2m} and i_{x2m} of a Fourier expansion of J_{x2} are therefore proportional to I_m and i_m, respectively. These coefficients are determined from a least squares fit to the measurements $\bar{B}_j$, $j = 1, 18$ by minimising

$$\chi^2 = \sum_{j=1}^{18} (B_j - \bar{B}_j)^2 / (\Delta B_j)^2$$

via $\partial\chi^2/\partial I_m = 0$, where ΔB_j is the assumed error on measurement $\bar{B}_j$.

The value B_j calculated at the position of a pickup coil is

$$B_j = \sin \mu_j \left(-\frac{1}{R}\frac{\partial \psi}{\partial R} \right) - \cos \mu_j \left(\frac{1}{R}\frac{\partial \psi}{\partial R} \right),$$

where μ_j denotes the angle between the vessel normal n (Fig. 2) at (R_j, Z_j) and $Z = 0$. The error ΔB_j is

$$\Delta B_j = \varepsilon_j \langle B \rangle \qquad \text{or} \qquad \Delta B_j = \varepsilon_j B_j,$$

where ε_j is a fixed accuracy level ($\sim 2\%$). A typical value for χ^2 is $18 - M - 1 = 14$, corresponding to a good fit to the measurements. The solution $\psi(R, Z)$ is calculated on a polar grid of typically 24 azimuthal points by 20 radial points.

To determine ψ_p a check is made on whether an x-point (saddle-point) is present inside the vessel. This is carried out by a fast and approximate estimate of the Poincare index for a vector field. At 4 neighbouring points on the grid the following index is evaluated

$$P_x = (\mathbf{b}_1 \times \mathbf{b}_2) \cdot (\mathbf{b}_3 \times \mathbf{b}_4),$$

where $\mathbf{b}$ denotes a unit vector parallel to $\mathbf{B}$ and points 1, 2, 3, 4 connected clockwise form a closed rectangle. If $P_x < 0$ an x-point inside the rectangle is found by Taylor expansion and $\psi_p = \psi_x$. If $P_x > 0$, ψ_p is found from (4). The plasma boundary Γ_p is tracked, yielding 24 values of (R_p, Z_p) and B on Γ_p.

3.2. *Plasma Parameters*

From the variation of B on Γ_p several quantities can be calculated, e.g., the current moments Y_m of [11], the Shafranov integrals S_1, S_2 [14], and S_3 [15]. From the well known relations

$$\Lambda = \beta_I + \tfrac{1}{2} l_i = \tfrac{1}{2} S_1 + (1 - \tfrac{1}{2}\delta) S_2 \tag{5}$$

$$\beta_I - \mu = S_1 + \delta S_2, \tag{6}$$

two values of β_I are calculated; δ given in [14] is approximated as $1 - R_J/R_M$. From the diamagnetic flux (corrected for many effects [2]), μ is derived and β diamagnetic is found. A method of separating β_I and $\frac{1}{2} l_i$ [16] is applied by calculating l_i from

$$l_i = \frac{2K}{1 + K^2} (\tfrac{1}{2} + 0.357 \tilde{I}) \tag{7}$$

where

$$\tilde{I} = 5.8 \left(\frac{1}{2} - \frac{2 Y_2}{(1 - K^2) a^2} \right) \frac{2 \beta_I a^2 \Lambda}{R_M^2 (K^2 - 1)} \frac{5 + K^2}{4} \alpha_p.$$

The above expressions arise from an empirical fit of l_i calculated for a variety of equilibria of plasma elongation K, minor radius a, and $0 < \alpha_p < 1$ a pressure profile parameter; it can be seen that the separation of l_i and β_i becomes invalid as $K \to 1$; this has also been found in [5, 10, 15].

A global power balance is evaluated by estimating the flux inductance defined as

$$h_i = \frac{4\pi}{\mu_0 I R_0} \int_{R_0}^{R_p} B_z \, R \, dR,$$

where R_0 is the magnetic axis and R_p the boundary, both at $Z = 0$. The estimate yields

$$h_i = 1.2 \, l_i + 0.4$$

and is again based on an empirical fit. The loop voltage at the plasma boundary

$$V_p = -2\pi \frac{\partial \psi_p}{\partial t}, \tag{8}$$

where ψ_p is usually at the limiter position. If the plasma detaches from the limiter and moves to one of the "virtual" limiter points (Eq. 4), no account is taken of the advective term $\mathbf{V} \times \mathbf{B}$ as the movement is regarded as instantaneous.

The axial loop voltage is found from

$$V_0 = V_p + \frac{\partial}{\partial t}\left(\frac{1}{2} \mu_0 R_0 h_i I\right).$$

The Poynting flux through Γ_p becomes

$$P_Y = V_p I$$

and the Ohmic heating rate is derived from

$$P_\Omega = P_Y - \frac{\partial}{\partial t}\left(\frac{1}{4} \mu_0 R_0 l_i I^2\right). \tag{9}$$

The magnetic confinement time is

$$\tau_{EM} = \frac{W}{P_T - \partial W/\partial t}, \qquad W = \frac{3}{8} \mu_0 R_0 \beta_I I^2, \tag{10}$$

where the total power (Ohmic, RF, neutral beams) is

$$P_T = P_\Omega + P_{RF} + P_{NB}.$$

3. *Plasma Surface Representation*

The plasma surfaces between the boundary Γ_p and the magnetic axis are described by the formalism of Lao *et al.* [13]

$$\begin{aligned} R &= R_0(x) + ax\cos\chi + R_2(x)\cos 2\chi, \\ Z &= E(x)(ax\sin\chi - R_2(x)\sin 2\chi). \end{aligned} \tag{11}$$

The parameter χ runs from 0 to 2π throuth the relation $\chi = \theta + t\sin\theta$, $|t| < 1$. The above representation discards any asymmetry in Z which might be present in the measurements; a is the minor radius at $Z = 0$ such that $0 \leqslant x \leqslant 1$.

The functions $R_0(x)$, $R_2(x)$, $E(x)$ could be determined by the moment method [13]. At present the ellipticity and triangularity are given by

$$E(x) = e_0 + e_2 x^2 + e_4 x^4 \tag{12}$$

$$R_2(x) = R_{21} x^4. \tag{13}$$

The shift function for $l_i \leqslant 0.8$ is given by [17]

$$R_0(x) = R_{01} + \frac{a^2}{2R_{01}} \frac{(E_1^2+1)}{3E_1^2+1}\left(\beta_I + \frac{1}{4} + \frac{1}{4}\frac{E_1^2-1}{3E_1^2+1}\right)(x^2-1) \tag{14a}$$

and for $l_i > 0.8$ it is given by

$$\begin{aligned} R_0(x) = R_{01} &+ \frac{a^2}{2R_{01}(3E_1^2+1)} \frac{3E_1^2-1}{4}(1-x^2) \\ &+ (E_1^2+1)\left(\beta_I + \frac{1}{6}\right)\left(1 - \frac{x^2}{2-x^2}\right) + \frac{1}{3}(E_1^2+1)\log(2-x^2). \end{aligned} \tag{14b}$$

In order to find the coefficients in the above expressions a parabolic spline is fitted through the points (R_j, Z_j), $j = k-1, k, k+1$, where Z_k is the maximum Z of the calculated boundary points. The maximum value of the parabolic spline is used to determine R_{21} from a cubic equation; $E_1 = E(x=1)$ is also found.

Since from (12) $E_1 = e_0 + e_2 + e_4$, we have two free parameters in the ellipticity function. At present only one is used and supplied as input; calculations with the full equilibrium code (Blum *et al* [10]) carried out for a variety of equilibria allow for an estimate of e_0.

Figure 3 shows the geometry of plasma surfaces described by (11) together with the calculated plasma boundary of Fig. 2. Also shown are the locations of some diagnostic sightlines. For comparison we show in Fig. 4 the plasma surfaces calculated for the same data using the equilibrium method developed by J. Blum *et al.* [10]. The analysis described in the next section assumes temperature and density to be constant on a plasma surface. For this analysis two Jacobians are required:

$$\omega(x) = \int_0^{\pi} \tau\, dx, \qquad \Omega(x) = \int_0^{2\pi} R\tau\, dx, \tag{15}$$

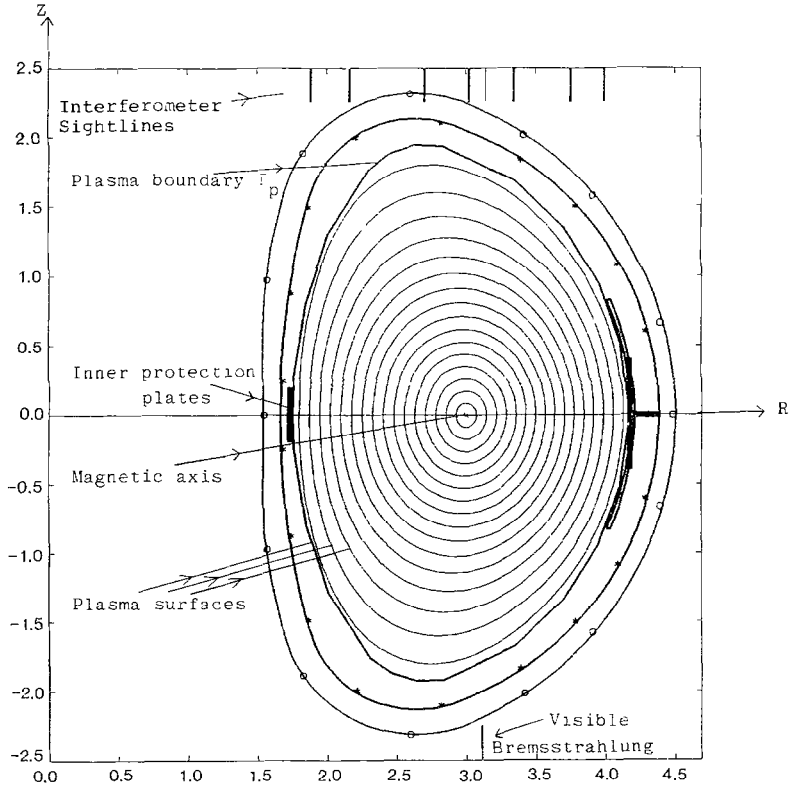

FIG. 3. JET vessel geometry with locations of diagnostic sightlines marked. The plasma surfaces (Section 3.2) are derived from the boundary Γ_p and other plasma parameters. This surface geometry is used in the analysis.

where

$$\tau = \frac{\partial R}{\partial x}\frac{\partial Z}{\partial x} - \frac{\partial R}{\partial x}\frac{\partial Z}{\partial x}.$$

The functions (15) are readily found using (11).

$$\begin{aligned} \omega(x) &= 2\pi \frac{d}{dx}\left(E(x)\left(\frac{1}{2}a^2x^2 - R_{21}^2(x)\right)\right) \\ \Omega(x) &= 4\pi^2\left(R_0(x)\,\omega(x) + \omega(x)\frac{d}{dx}R_0(x)\right). \end{aligned} \tag{16}$$

This solution concludes the first stage. In the integrated analysis a few more quantities not mentioned here are calculated. The calculations described in this section are carried out by the computer code FAST for 1000 time slices (discrete time

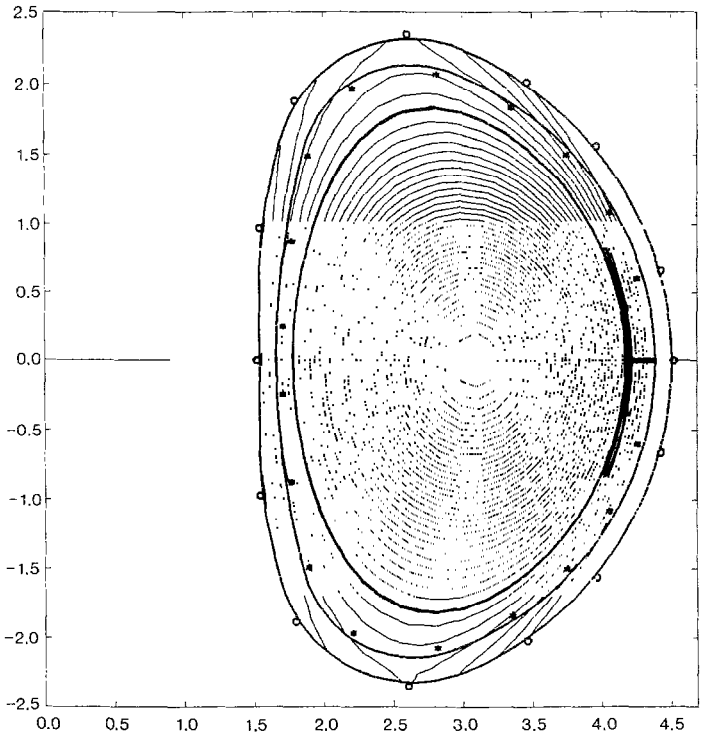

FIG. 4. JET vessel with plasma surface from the full equilibrium solution obtained by the code IDENTB [10].

values). Time derivatives such as in Eq. (7)–(10) are evaluated by a "running average technique" well known in the field of data manipulation; we form the average

$$\bar{f}(t) = \frac{1}{2\,\Delta T} \int_{t-\Delta T1}^{t+\Delta T2} f(t')\, e - \frac{(t-t')^2}{2\sigma^2}\, dt'. \tag{17}$$

and use $\partial f/\partial t = \partial \bar{f}/\partial t$. For the JET data we have used $\Delta T_1 = \Delta T_2 = 0.2$ s and $\sigma \to \infty$; presently $\Delta T1 = 0.1$ s and $\Delta T2 = 0$. The analysis described up to this point is carried out by FAST and consumes 65–75 s of IBM 3083 CPU time.

4. Analysis of JET Diagnostic Data

Using the plasma surface topology described in the previous section we carry out an analysis of data from the diagnostics listed in Table I. The aim of the analysis is to *globally* assess the time evolution of confinement of particles and energy, impurity content, profiles of temperatures and density. In doing so, the following

assumptions are made partly because of lack of detailed information and partly to speed up the calculation:

(i) Plasma density and temperature are constant on a surface.

(ii) Z_{eff} is uniform in space (but not in time).

(iii) Ion density and temperature profiles are similar to those of the electrons.

The analysis runs through the following stages:

1. The electron temperature profile $T_e(x)$ from electron cyclotron emission.
2. The total radiation power from bolometer data.
3. The axial ion temperature T_{io} from neutral particle analyser data.
4. The electron density profile $n_e(x)$ from a fit to interferometer channel values.
5. The axial ion temperature T_{io} from neutron emission.
6. Z_{eff} from visible Bremsstrahlung emission.
7. Particle confinement time from $n_e(x)$ and H_α emission at the wall and limiter.
8. Z_{eff} (resistive) by integration of Ohm's law.
9. Confinement of energy.

Stages 1–3 are calculated by the three interpretation codes ECM1, BOLO, NPA3, respectively. Their results are used in stages 4–9 by the analysis code INDIANA, which will be briefly described in the folllowing.

4.1. *Density Profile Fitting*

The electron density profile is assumed to be of the form

$$n_e(x) = (n_0 - n_w)(1 - x^2)^\gamma + n_w. \tag{18}$$

The axial value n_0, the edge value n_w and the peakedness γ are determined by minimising

$$\chi^2 = \sum_{j=1}^{8} \left(\frac{N_j - \bar{N}_j}{\Delta N_j} \right)^2,$$

where N_j denote the 8 chord measurements from 2 interferometers. The calculation of N_j involves the determination of intersection between vertical sightlines and adjacent plasma surfaces. These are found by a fast direct, i.e., non-iterative method. The minimisation involves a non-linearity via γ and the values are found by an iteration procedure in which, for fixed γ_k, linear equations are solved for n_0 and n_w. The value γ_{k+1} at the next iteration is estimated from a Taylor expansion of $\chi^2(\gamma)$; the minimum is found when $\partial\chi^2/\partial\gamma$ changes sign. This procedure is found to be very fast and requires an average of 2 iterations for each time slice; only

during rapid density or density profile changes caused by auxiliary heating may more iterations be recorded. For an assumed error $\Delta N_j = 0.02\,\bar{N}_j$, the values of χ^2 range from 3–10. Typically 51 plasma surfaces are used.

4.2. Z_{eff}

From the vertical chord measurement of visible Bremsstrahlung emission B_v at wavelength λ we find the value of Z_{eff} from

$$Z_{\text{eff}} = \frac{4\pi\lambda B_v}{9.5\ 10^{-35}} \frac{1}{I_v}, \tag{20}$$

where $I_v = \int n_e^2 g_{ff} T_e^{-1.2}\, dz$, the integration being taken along the viewed line; the intersections between this line and the plasma surfaces are found as in the previous sections. The gaunt factor g_{ff} varies in a JET discharge from 1 at the edge to approximately 4 in the centre; more details are given in [2].

4.3. *Particle Confinement*

An edge or global particle confinement time τ_p is calculated from

$$\tau_p = \frac{N_e}{\phi_L + \phi_W + \phi_i + \phi_G - dN_e/dt}. \tag{21}$$

The fluxes ϕ in (21) are from limiter (L), wall (w), impurity (i) and gas feed + natural beam injection (G). ϕ_L and ϕ_W are related to H_α emission measurements and ϕ_i is related to these two hydrogenic fluxes as well as Z_{eff}. The total particle inventory N_e is given via $n(x)$.

4.4. *Central Ion Temperature*

The total D – D reaction rate from the neutron producing branch is given by

$$R_n = \int n_D^2 \langle \sigma v \rangle\, C_D\, dv. \tag{22}$$

The deuterium density is $n_D = f_D n_e$ (f_D constant in space) and C_0 is the neutron detector efficiency function which is surface averaged via

$$\langle C_D(R, Z) \rangle = C_D(x).$$

The ion temperature on axis T_{io} is found by iterating on

$$\frac{1}{R_n}\frac{\partial R_n}{\partial T_{io}} = \frac{1}{\langle \sigma v \rangle}\frac{\partial \langle \sigma v \rangle}{\partial T_{io}}.$$

This equation determines δT_{io} from $\delta R_n = R_n - R_{\text{meas}}$. Usually only 2 iterations are required except when T_{io} changes rapidly during onset of RF heating. The deuterium fraction f_D is supplied as input and may vary according to vessel conditions.

4.5. Z_{eff} *from Resistivity*

Integration over the plasma cross section of Ohm's law in the approximate form $J_\phi = \sigma_{11} E_\phi$ yields 3 estimates of Z_{eff} depending on the choice of resistivity. These estimates are referred to as the axial, the Spitzer or the neo-classical values corresponding to σ_{11} being given by the Spitzer formulae or σ_{11} being neo-classical. Further details are given in [2].

4.6. *Confinement of Energy*

The energy content of electrons and ions are

$$W_k = \frac{3}{2} \int_0^1 p_k(x)\, \Omega(x)\, dx, \tag{23}$$

where k indicates either electrons (e) or ions (i), and p denotes pressure nkT. The poloidal beta value is

$$\beta = \frac{32\pi R_0 a_0^2}{3\mu_0 I^2 R_M} (W_e + W_i). \tag{24}$$

A global energy ($W = W_e + W_i$) confinement time is defined as

$$\tau_E = \frac{W}{P_\Omega + P_{RF} + P_{NB} - dW/dt}. \tag{25}$$

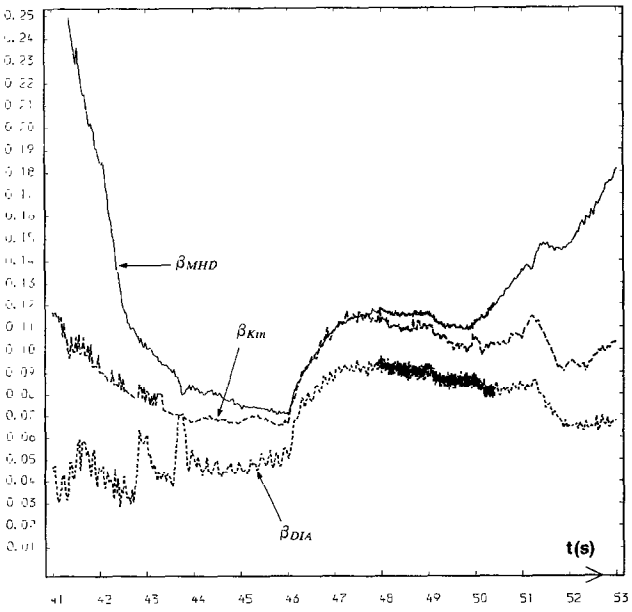

FIG. 5. Time evolution of plasma β for JET discharge No. 7118 with neutral beam heating. The curves are marked β_{MHD} (Eq. (5) and (7)), β_{DIA} (Eq. (6)), and β_{Kin} (Eq. (23) and (24)).

In this expression P_{RF} and P_{NB} denote the total RF power and total neutral beam power delivered to the plasma.

The analysis carried out by INDIANA consumes 45–50 s of IBM 3083 time.

5. Representative Results from JET Pulses

As mentioned earlier, representative results from the analysis described in this paper are produced as graphs after each JET pulse. Figure 5 shows for one pulse the temporal evolution of the plasma beta: β_{MHD} determined from Eq. (5) and (7); β_{DIA} from Eq. (6); and β_{kin} found from the spatial integration in equations 23 and 24. Figure 5 shows that all 3 estimates of β increase as NB power is applied to the plasma. Figure 6 shows the time dependence of the electron temperature determined by electron cyclotron emission and two estimates of the ion temperature; one based on the neutron yield (Section 4.4) and one based on neutral particle analyzer data. Figure 7 shows the energy confinement times defined by Eq. (10) and (25) and the particle confinement time defined by Eq. (21). Figure 8 shows the variation of

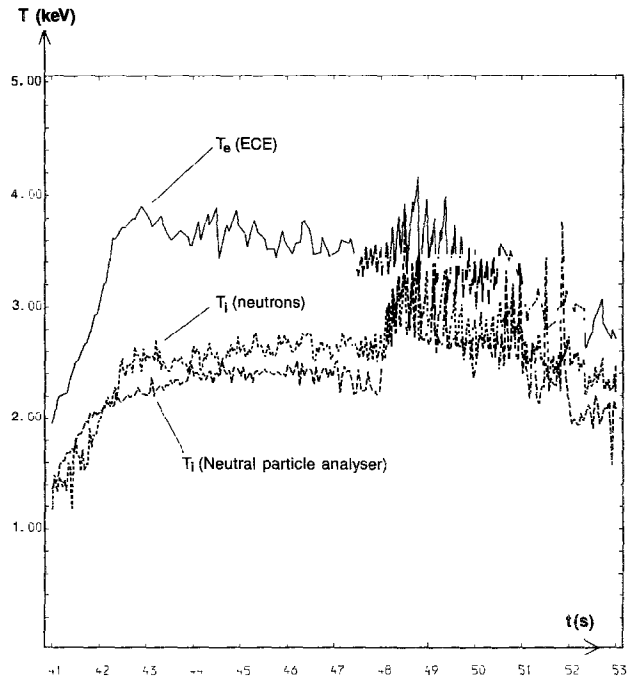

FIG. 6. Time evolution of central values of electron temperature and ion temperature for JET discharge No. 7118. The curves are marked T_e (ECE), T_i (neutron yield), T_i (neutral particle analyser). The neutral beam power of 4 MW is applied between $t = 48$ s and $t = 50$ s. The data sampling rate is increased and so are the sawtooth oscillations during the beam heating period.

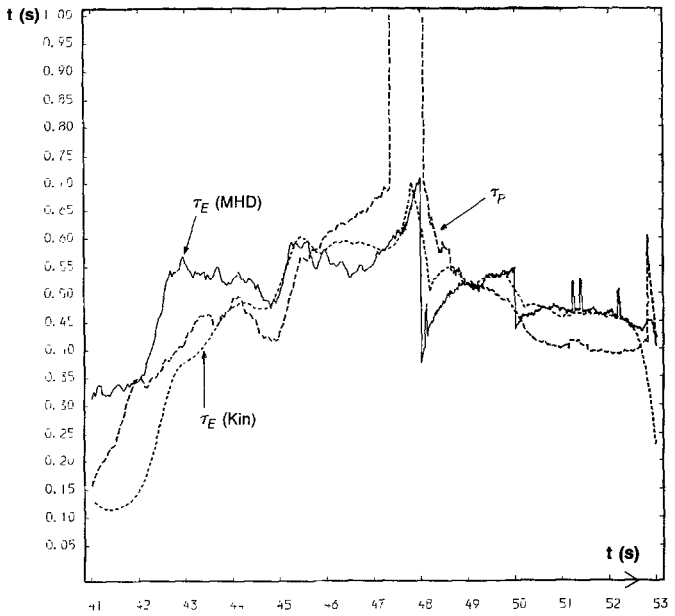

FIG. 7. Time variation of energy and particle confinement times for JET discharnge No. 7118. There is a drop in τ_E as the neutral beam power is applied. The short increase in τ_p before beam power is applied is due to a drop in the flux from the limiter.

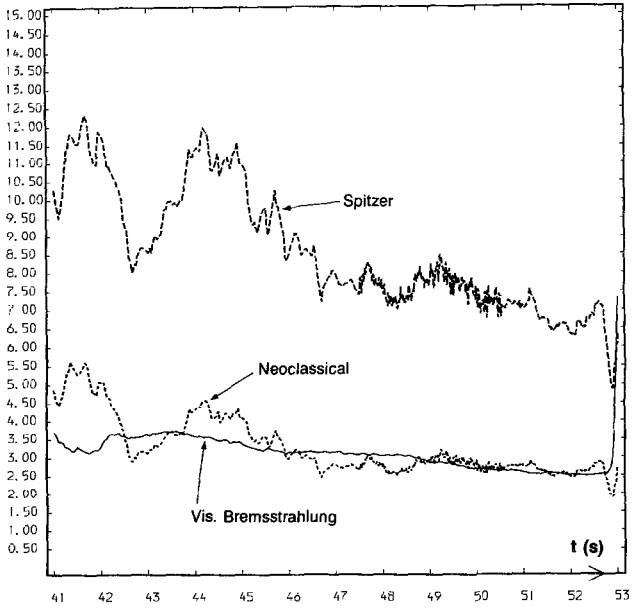

FIG. 8. Time variation of Z_{eff} as determined by the methods of Sections 4.2 and 4.5. The estimate based on a neoclassical resistivity agrees reasonably well with that based on visible bremsstrahlung (JET discharge No. 7118).

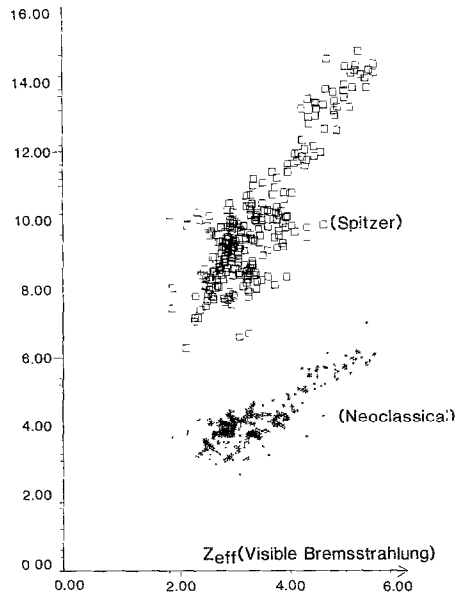

FIG. 9. The values of Z_{eff} derived from Spitzer resistivity (squares) and from neoclassical resistivity (asterisks) plotted against Z_{eff} determined from visible bremsstrahlung. Each square and asterisk represent a single time value from a JET pulse.

assuming a neoclassical resistivity is in reasonable agreement with the value determined from visible bremsstrahlung; this is usually the case for JET. All the graphs in Fig. 5–8 are taken from calculations on data from the same JET pulse number 7118; the values on the time axes Fig. 5–8 correspond to plasma breakdown and start of current at time = 40 s. Figure 9 shows results from calculations on well over 1000 pulses. Each square or asterisk represents a single time point value from one pulse Z_{eff} (neoclassical, asterisks) and Z_{eff} (Spitzer, squares); these values are plotted against the corresponding values of Z_{eff} (bremsstrahlung). Figure 10 represents the results of a regression analysis on τ_E (Eq. (25)) in which a best fit is produced relating τ_E to other plasma parameters [18]. Each point in Fig. 10 represents a single time value from one pulse and these values as well as those of Fig. 9 have been extracted from a summary data bank as mentioned in Section 1. The different symbols in Fig. 10 refer to various discharge types. Graphs like those of Fig. 9 and 10 are produced regularly to check for data inconsistencies as well as to study genuine changes in plasma parameters; for exemple, a sudden change in Z_{eff} from one day to another for similar pulses may be due to a change in the vacuum vessel wall condition, e.g., by carbon desposits. A different energy confinement scaling law may emerge as new operating regimes are explored; references [18, 19] illustrate such a trend occurring from 1984 to 1985.

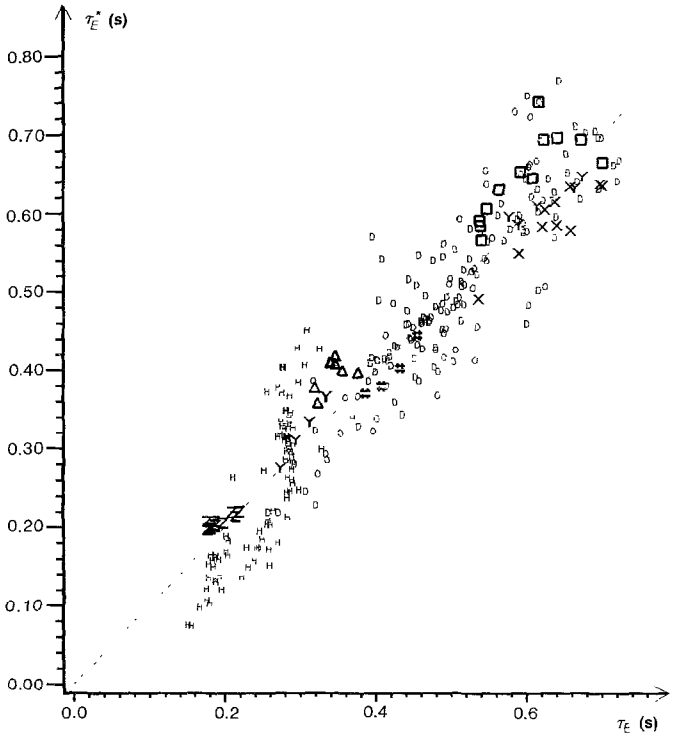

FIG. 10. Result of a regression analysis in which τ_E is plotted against τ_E^* where [18] $\tau_E^* = 0.013 B_\phi^{0.57} q^{0.33} n_e^{0.38} K^{0.2} R^{3.2} \varepsilon^{1.7} A^{0.6}$. In this expression the symbols denote; toroidal field, safety factor, density, elongation, major radius, inverse aspect ratio (a/R), and atomic mass, respectively. The different symbols on the plot refer to a variety of JET discharges.

6. Features of Analysis Codes

The two analysis codes FAST and INDIANA mentioned in the Introduction both contain a large number of identically structured packages (or modules). Some of these packages carry out quite trivial tasks such as reading data or results into certain data areas (common blocks). Other packages like the fast equilibrium package [12] perform complete calculations on data. To establish a set of standards for the data communication between packages and for the reliable operation of these packages was one of the major tasks to be solved before JET began operation in June 1983. In addition, the analysis code FAST had to execute a real time program on the JET experimental console computer (a NORD-570). As diagnostics were added to JET, new packages were required and the resulting changes to existing programs and packages could have necessitated a monumental software effort. In consultation with K. Roberts and M. L. Watkins of JET it was decided to adapt the OLYMPUS system [1] for a sequence of packages integrating

JET data. The essential features of this adaptation can be summarised as follows (details will be given elsewhere):

A. Each package is structured like an OLYMPUS program with sub-routines belonging to classes 1–4 as described in [1].

B. Each package has a standard "plug in" control sub-routine which can transfer control to any of the sub-routines of the package using a "digital" dialling code [1], e.g., CALL DENNEX (1, 4, 1) will call subroutine 1.4 of package DENNEX (density profile fitting).

C. Each package is associated with a number, e.g., DENNEX is number 2.15 or 215.

D. All sub-routines in a package have names ending with the same 3 letters, e.g., NEX for package DENNEX. All the results have FORTRAN variable names ending with those letters. As an example the FORTRAN variable AXNEX is an array combining 1000 values of the electron density on axis; these values are stored in PPFs under that same name and that name is also retained when values are extracted into the summary data bank.

The assembly of several packages into an interpretation code like FAST is facilitated by the use of two multiplexor sub-routines. The first one can transfer execution control to any of the "plug in" control sub-routines (under B). To carry out a standard task, e.g., reading namelist variables for all packages, a single call is made to the multiplexor routine with the arguments (1, 4, 1) [1]; all packages hooked up to the multiplexor will then carry out the reading of namelists. A second multiplexor routine is used for the data flow and communication. This routine is called by all packages and has as arguments an array starting address and an identifier of 24 characters. All the I/O from PPF files go through this multiplexor. Each individual variable can be reached for plotting, printing (I/O), etc. by a dialling code similar to that of the telephone system in the U.S.A. The dialling code for the variable AXNEX is 215 5502; 215 is the package number (area), 55 is the common block number (exchange), and 02 is the variable number (subscriber). Standard dialling rules [1] are used to access the whole block via 215 5500, or all blocks if necessary via 2150000.

The implementation of these features may seem extravagant, perhaps unnecessary. However, during the development of the various packages used by the interpretation codes, a large number of modification extensions have been implemented and changes are still in progress. A clear division of the computational tasks involved in the interpretation of the data is clearly of great help when it comes to either changes to the FORTRAN coding or to changes in the structure of the data.

Many more features than those mentioned here derive from the work of Keith Roberts and the first article in *Computer Physics Communication* [20] describes some of the guiding principles which have been embodied in many scientific computer programs.

ACKNOWLEDGMENTS

The philosophy behind the data processing, data flow and code structure owes much to the late Keith Roberts. The implementation owes much to the scientists at JET. The author would like to express his [illegible] J. O'Rourke (plasma density), D. J. Campbell (ECE), G. Tonetti (diamagnetic loop), M. Brusati (neutral particle analyser), E. Lazzaro (equilibrium).

REFERENCES

1. K. V. ROBERTS, *Comput. Phys. Commun.* **1**, 237 (1974); J. P. CHRISTIANSEN AND K. V. ROBERTS, *Comput. Phys. Commun.* **1**, 245 (1974).
2. R. T. ROSS, JET Internal Note JDN/T(85)1, to be published as a JET report; J. P. CHRISTIANSEN, JET Report JET-R(86)04, 1986 (unpublished).
3. R. J. GOLDSTON *et al, J. Comput. Phys.* **43**, 61 (1981).
4. D. W. SWAIN AND G. H. NEILSON, *Nucl. Fusion* **18**, 1015 (1982).
5. J. L. LUXON AND B. B. BROWN, *Nucl. Fusion* **18**, 813 (1982).
6. K. SHINYA AND H. YOKOMIZO, General Atomic Report GA-A16750, 1982 (unpublished).
7. L. L. LAO, H. ST. JOHN, R. D. STAMBAUGH, A. G. KELLMAN, AND W. PFEIFFER, GA Technologies Report GA-A 17910, 1985; *Nucl. Fusion*, in press.
8. D. K. LEE AND Y. K. M. PENG, *J. Plasma Phys.* **25**, 161 (1981).
9. YU. K. KUZNETSOV AND A. M. NABOKA, *Sov. J. Plasma Phys.* **7**, 474 (1981).
10. *Proceedings, Second Workshop on Computational Problems in the Calculation of MHD Equilibria, Comput, Phys. Rep.* **1**, 345 (1984).
11. L. E. ZAKHAROV AND V. D. SHAFRANOV, *Sov. Phys. Tech. Phys.* **18**, 151 (1973).
12. W. FENEBERG, K. LACKNER, AND P. MARTIN, IPP Report 1/223, 1983 (unpublished).
13. L. L. LAO, S. P. HIRSHMAN, AND R. M. WIELAND, *Phys. Fluids* **24**, 1431 (1981).
14. V. D. SHAFRANOV, *Plasma Phys.* **13**, 757 (1971).
15. L. L. LAO, H. ST. JOHN, R. D. STAMBAUGH, AND W. PFEIFFER, GA Technologies Report GA-A17611, 1984; *Nucl. Fusion*, in press.
16. J. G. CORDEY, E. LAZZARO, P. STUBBERFIELD, P. THOMAS, AND M. L. WATKINS, Workshop on Transport Analysis Codes, PPPL, March 1984.
17. T. STRINGER. private communication (1984).
18. J. G. CORDEY *et al.*, 10th IAEA Conference on Plasma Physics and Controlled Nuclear Fusion Research, London, September 1984, Paper AEA-CN-44/A-III-3.
19. R. J. BICKERTON *et al.*, 12th European Conference on Controlled Fusion and Plasma Physics, Budapest, September 1985.
20. K. V. ROBERTS, *Comput. Phys. Commun.* **1**, 1 (1969).